Society of Medical Education & Research

2023, Volume 3, Issue 2, Page No: 48-68

ISSN: 3108-4834

Archive of International Journal of Cancer and Allied Science

CircPHLPP2 Facilitates Colorectal Cancer Progression and Anti-PD-1 Resistance via ILF3-Mediated Regulation of IL36γ Transcription

Alexei Sergeyevich Volkov[1]*, Dmitry Igor Kuzmin[1]

[1]Department of Oncology, Pirogov Russian National Research Medical University, Moscow, Russia.

***E-mail** ✉ a.volkov.pirogov@yahoo.com

Abstract

Most patients with colorectal cancer (CRC) show a poor response to anti-programmed cell death protein 1 (PD-1) therapy, and the mechanisms behind this resistance are not well understood. Circular RNAs (circRNAs) have been recognized as key regulators in tumor development and progression, with potential utility in cancer detection and predicting therapeutic outcomes. Despite this, the involvement of circRNAs in immune evasion in CRC remains largely unexplored.CircPHLPP2 was initially identified through circRNA microarray analysis. Its expression in colorectal cancer patients and correlation with clinical parameters were evaluated by RT-qPCR. To determine its functional role, cell proliferation and colony formation assays, in vivo subcutaneous tumor models, and multicolor flow cytometry were conducted. Downstream signaling pathways influenced by circPHLPP2 were investigated using RNA sequencing, RT-qPCR, and Western blot analyses. Finally, RNA pull-down, RNA immunoprecipitation (RIP), and immunofluorescence assays were employed to uncover proteins interacting with circPHLPP2.CircPHLPP2 is upregulated in colorectal cancer patients who display resistance to anti-PD-1 therapy. It markedly promotes CRC cell proliferation and tumor growth, whereas silencing circPHLPP2 enhances the therapeutic effect of anti-PD-1 in vivo. Mechanistically, circPHLPP2 directly interacts with ILF3, promoting its accumulation in the nucleus and subsequently increasing IL36γ transcription. This cascade diminishes NK cell infiltration and suppresses their IFN-γ production and granzyme B, ultimately facilitating tumor progression.In summary, our study uncovers a previously unrecognized mechanism through which a circRNA mediates immune evasion in colorectal cancer. CircPHLPP2 holds potential as both a therapeutic target and a prognostic biomarker for CRC patients.

Keywords: Colorectal cancer, CircPHLPP2, Immune evasion, NK cell

Introduction

Colorectal cancer (CRC) is the third most frequently diagnosed malignancy and ranks second among causes of cancer-related deaths worldwide [1]. Limited therapeutic options severely impact both survival outcomes and quality of life for patients with advanced CRC [2]. The development of immune checkpoint inhibitors (ICIs), including programmed cell death protein 1 (PD-1) blockers, has offered new strategies for treating advanced disease. Clinical evidence shows that pembrolizumab, a humanized monoclonal antibody against PD-1, significantly prolongs survival in CRC patients with microsatellite instability-high or deficient mismatch repair (MSI-H/dMMR) [3]. However, patients with microsatellite stable or proficient mismatch repair (MSS/pMMR), who make up the vast majority of CRC cases (~95%) [4], generally fail to respond to ICI monotherapy [5]. Encouragingly, the REGONIVO trial reported that combining anti-PD-1 therapy with tyrosine kinase inhibitors (TKIs) can yield favorable responses in metastatic MSS/pMMR CRC [6]. Despite these advances, biomarkers to predict anti-PD-1 efficacy in MSS/pMMR CRC are still lacking. Therefore, elucidating the molecular basis of immunotherapy

Access this article online https://smerpub.com/

Received: 23 March 2023; **Accepted:** 19 July 2023

How to cite this article: Volkov AS, Kuzmin DI. CircPHLPP2 Facilitates Colorectal Cancer Progression and Anti-PD-1 Resistance via ILF3-Mediated Regulation of IL36γ Transcription Arch Int J Cancer Allied Sci. 2023;3(2):48-68. https://doi.org/10.51847/HMsHY9e0OQ

resistance is crucial for identifying new predictive markers and therapeutic targets, which may ultimately improve patient outcomes.

Circular RNAs (circRNAs) are covalently closed, single-stranded RNA molecules that are broadly expressed yet show tissue-specific patterns in humans [7]. Many circRNAs are aberrantly expressed in CRC tissues, cells, blood, and exosomes, influencing tumor initiation, metastasis, and resistance to chemotherapy [8, 9]. Emerging studies suggest that circRNAs also modulate the tumor microenvironment and contribute to immune evasion [10, 11]. For instance, exosome-derived CircCCAR1 induces $CD8^+$ T-cell dysfunction by stabilizing PD-1, promoting anti-PD-1 resistance in hepatocellular carcinoma [12], while CircDLG1 facilitates gastric cancer progression and anti-PD-1 therapy resistance by upregulating CXCL12 [13]. Nevertheless, the role of circRNAs in driving immunotherapy resistance in CRC remains poorly characterized. Given their stability and detectability in body fluids, circRNAs also present potential as predictive biomarkers for anti-PD-1 responsiveness. Identifying circRNAs that regulate immune escape in CRC is therefore of significant interest.

NK cells are innate immune effectors capable of detecting and eliminating tumor cells without prior sensitization [14]. In addition to direct cytotoxicity via perforin or antibody-dependent cell-mediated cytotoxicity (ADCC), NK cells secrete cytokines and chemokines to recruit and activate T cells, bridging innate and adaptive immunity [15, 16]. Tumors can evade NK cell-mediated immunity through multiple mechanisms, such as increasing inhibitory receptors like PD-1 on NK cells [17]. Blocking PD-1/PD-L1 interactions has been shown to enhance NK cell activity, highlighting their crucial role in the success of immunotherapy [18]. Moreover, higher NK cell abundance in circulation or tumor tissues is correlated with reduced metastasis and better prognosis across various cancers, including CRC [17, 19]. Despite their importance, the contribution of NK cells to anti-PD-1 resistance in CRC remains insufficiently understood.

In this study, we identified circPHLPP2 as a circRNA highly expressed in CRC tissues, associated with poor prognosis and resistance to anti-PD-1 therapy. Mechanistically, circPHLPP2 binds ILF3 to promote IL36γ transcription, resulting in reduced NK cell infiltration and impaired granzyme B and interferon-γ (IFN-γ) production, thereby facilitating tumor progression. Importantly, silencing circPHLPP2 enhanced the anti-tumor efficacy of PD-1 blockade, highlighting circPHLPP2 as a promising prognostic biomarker and potential therapeutic target in CRC immunotherapy.

Materials and Methods

Human tissues

Tissue specimens, including both fresh-frozen and paraffin-embedded samples, were collected from pMMR CRC/metastatic MSS patients treated with PD-1 inhibitors at Sun Yat-sen University Cancer Center between August 2019 and October 2022. These patients had undergone either colonoscopic biopsies or palliative surgery. Treatment response was assessed according to RECIST 1.1 criteria. Overall survival (OS) was calculated from the initiation of anti-PD-1 therapy to either the date of death from any cause or the last follow-up. For immunohistochemical analyses, 381 formalin-fixed, paraffin-embedded CRC samples, along with corresponding clinicopathological data, were obtained from patients treated between January 2007 and December 2012, with all patients providing informed consent. OS in this cohort was defined as the interval from surgery to death or last follow-up.

CircRNA microarray profiling

To uncover circRNAs associated with resistance to anti-PD-1 therapy, we performed microarray analyses on tumor and matched adjacent normal tissues from 18 patients: 8 who exhibited partial response (PR) and 10 who showed progressive disease (PD) following anti-PD-1 treatment. CircRNA enrichment was achieved by digesting linear RNAs with RNase R. The enriched circRNAs were then amplified and labeled with fluorescent cRNA using the Arraystar Super RNA Labeling Kit via random priming. Hybridization was performed on the Human circRNA Array V2 (8 × 15 k, Arraystar), and arrays were scanned with an Agilent G2505C Scanner. Data extraction and initial processing were conducted with Agilent Feature Extraction software (version 11.0.1.1), followed by quantile normalization and statistical analysis using R software.

Cell transfection and plasmid

The overexpression construct for hsa_circ_0003681 (human circPHLPP2) was generated using the pLC5-ciR backbone by GeneSeed (Guangzhou, China), while the

EIF4A3 overexpression plasmid (pLVX vector) was produced by Tsingke Biotech (Beijing, China). Custom-designed small interfering RNAs (siRNAs) targeting EIF4A3, HNRNPC, U2AF2, and corresponding negative controls were purchased from Genecefe (Jiangsu, China). SiRNAs targeting ILF3 (si-ILF3) and non-targeting control siRNAs (si-NC) were obtained from Public Protein/Plasmid Library (Nanjing, China). Short hairpin RNAs (shRNAs) against hsa_circ_0003681, mmu_circ_0014549 (mouse circPhlpp2), and mouse IL36γ, along with their respective controls, were synthesized by GeneChem (Shanghai, China). Lentiviral particles carrying mmu_circ_0014549 or control sequences were produced by GenePharma (Shanghai, China). Transfections and lentiviral infections were performed following manufacturer protocols and previously reported procedures [20].

Immunohistochemistry (IHC)

IHC staining was conducted according to standard procedures described previously [21]. Paraffin-embedded sections were deparaffinized, rehydrated, and treated with 3% H_2O_2 for 10 minutes to block endogenous peroxidase activity. Antigen retrieval was performed in a pressure cooker using either sodium citrate buffer or EDTA at sub-boiling temperature for 10 minutes. Sections were then blocked with 10% fetal bovine serum (FBS) for 1 hour at room temperature, incubated overnight at 4 °C with primary antibodies, and subsequently treated with biotinylated secondary antibodies for 1 hour at room temperature. The primary antibodies included anti-IL36γ (1:200, Abclonal) and anti-NKp46 (3 μg/mL, R&D). Hematoxylin was used for nuclear counterstaining. Staining intensity was graded on a scale from 0 (negative) to 3 (strong), and cumulative scores were calculated by multiplying intensity scores with the proportion of positive cells.

Flow cytometry

Tissue samples were digested in serum-free RPMI 1640 containing collagenase IV (0.2 mg/mL, Sigma-Aldrich) and DNase I (0.05 mg/mL, Roche), followed by mechanical dissociation using a gentle MACS Octo Dissociator (Miltenyi Biotec, Germany) to obtain single-cell suspensions. Immune cells were enriched via Percoll gradient centrifugation and stained with Zombie dye (1:500, Biolegend) and appropriate surface antibodies (1:200). For intracellular protein detection, cells were pre-stimulated with Cell Stimulation Cocktail (eBioscience) for 4 hours, followed by intracellular staining (1:100). Data acquisition was carried out on a CytoFlex flow cytometer (BD Biosciences, USA) and analyzed using FlowJo V10 (FlowJo LLC).

RNA Immunoprecipitation (RIP)

RIP assays were performed using the Magna RIP RNA-Binding Protein Immunoprecipitation Kit (Millipore). Antibodies were pre-incubated with magnetic beads at room temperature for 30 minutes. Anti-ILF3 (5 μg, Proteintech) and anti-EIF4A3 (5 μg, Proteintech) antibodies were used for pulldown, with IgG serving as the negative control. Cells were lysed in RIP buffer containing protease and RNase inhibitors, and lysates were incubated with antibody-conjugated beads overnight at 4 °C with gentle rotation. RNA associated with immunoprecipitated complexes was extracted and analyzed by RT-qPCR, normalized to input RNA.

GST pull-down

Interactions between circPHLPP2 and RNA-binding proteins were assessed using an MS2-tagged circRNA pull-down strategy [22]. Cells were co-transfected with MS2-circPHLPP2 or control MS2 plasmids and MS2-MCP-GST plasmid using Lipofectamine 3000. All plasmids were synthesized by GeneChem (Shanghai, China). Forty-eight hours post-transfection, cells were lysed in RIPA buffer, and the circPHLPP2-MS2-MCP-GST complexes were captured using Glutathione Sepharose 4B beads (ThermoFisher). Captured complexes were subsequently analyzed by RT-qPCR, western blotting, or mass spectrometry as needed.

Immunofluorescence and Fluorescence In Situ Hybridization (FISH)

FISH experiments were carried out using the SA-Biotin system (GenePharma, Shanghai, China) following the manufacturer's protocol. Cy3-labeled probes specific for circPHLPP2 were custom-designed by GenePharma. HCT116 cells were first fixed and permeabilized, then prehybridized to prepare for probe binding. Cells were incubated with the Cy3-labeled probes in hybridization solution overnight at 37 °C. After washing six times with Buffer C, cells were blocked with PBS containing 1% BSA and 0.05% Triton X-100 for 30 minutes at room temperature. Subsequently, cells were incubated with primary antibodies at 1:100 dilution for 1 hour at room temperature, followed by secondary antibodies conjugated to Alexa Fluor 488 (1:500, Invitrogen) for 45

minutes at 37 °C. Nuclei were stained with DAPI (1:1000, GenePharma) for 15 minutes at room temperature. Confocal images were acquired using an LSM880 microscope (ZEISS, Germany).

In vivo tumor formation

BALB/c Nude, NSG, BALB/c and C57BL/6J mice were sourced from Vital River (Beijing, China). Subcutaneous tumor models were established by injecting CRC cells into the right flank: 1.5×10^6 MC38, 5×10^5 CT26, or 5×10^6 HCT116/RKO cells. Tumor growth was monitored every three days starting one week after injection, and tumor volume was calculated as $V = (\text{width}^2 \times \text{length})/2$. When tumors reached ~200 mm^3, tissues and blood were collected for flow cytometry. For treatment experiments, mice with tumors ~100 mm^3 were administered 50 µg anti-PD-1 (BioXcell) or PBS via intraperitoneal injection every three days. NK cells were depleted by injecting 100 µL anti-asialo-GM1 (Cell Biolabs) intraperitoneally in BALB/c mice once per week, or 75 µg anti-NK1.1 (BioXcell) via tail vein in C57BL/6J mice every three days, beginning one day prior to tumor inoculation. Mice were euthanized when predefined ethical endpoints were reached. Excised tumors were weighed, photographed, paraffin-embedded, and sectioned for further analysis.

Statistical analysis

Statistical evaluations were performed using GraphPad Prism 9.0 and SPSS 25.0. Comparisons between two groups were conducted with Student's t-tests, while multiple-group comparisons used chi-square tests. Survival analyses were generated using Kaplan-Meier curves, with significance assessed by the log-rank test. Statistical significance was defined as $^*P < 0.05$, $^{**}P < 0.01$, $^{***}P < 0.001$, and $^{****}P < 0.0001$.

Results and Discussion

High circPHLPP2 expression correlates with poor prognosis in Anti-PD-1–Resistant CRC patients

To explore circRNAs associated with the efficacy of anti-PD-1 therapy in MSS/pMMR CRC patients, we conducted a circRNA microarray analysis on 18 paired samples, including primary tumor tissues and adjacent normal tissues, from patients treated with anti-PD-1–based regimens. Within this cohort, 10 patients exhibited progressive disease (PD) according to RECIST 1.1 criteria [23] and were classified as resistant to therapy, while 8 patients achieved partial response (PR) and were considered responsive. Analysis of the microarray data revealed 94 circRNAs that were markedly upregulated in tissues from anti-PD-1–resistant patients **(Figure 1a**), whereas 65 circRNAs were significantly elevated in tumor tissues relative to adjacent normal tissues **(Figure 1b**). Intersecting these two sets identified hsa_circ_0003681, derived from the PHLPP2 gene, which we designated as circPHLPP2. Notably, its biological role has not been previously reported **(Figure 1c).**

We further investigated the clinical relevance of circPHLPP2 by measuring its expression via RT-qPCR in a cohort of 67 CRC patients receiving anti-PD-1 therapy. The results demonstrated that circPHLPP2 levels were significantly higher in anti-PD-1–resistant patients **(Figure 1d)** and in CRC tumor tissues compared with normal tissues **(Figure 1e),** confirming the reliability of the microarray findings. Patients were stratified into high and low circPHLPP2 expression groups based on the median expression value. Kaplan-Meier survival analysis revealed that patients with elevated circPHLPP2 expression exhibited shorter overall survival and poorer prognosis **(Figure 1f).** Collectively, these data suggest that circPHLPP2 may play a critical role in CRC progression and immune evasion.

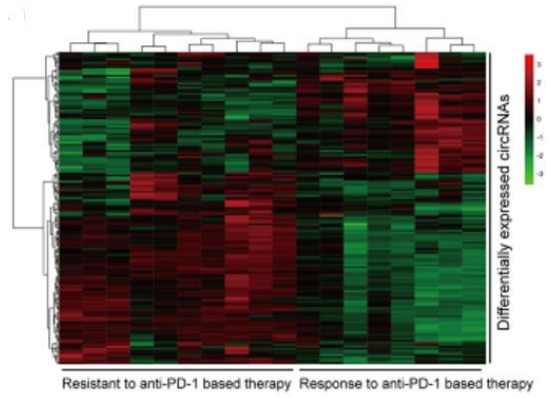
Differentially expressed circRNAs
Resistant to anti-PD-1 based therapy
Response to anti-PD-1 based therapy

a)

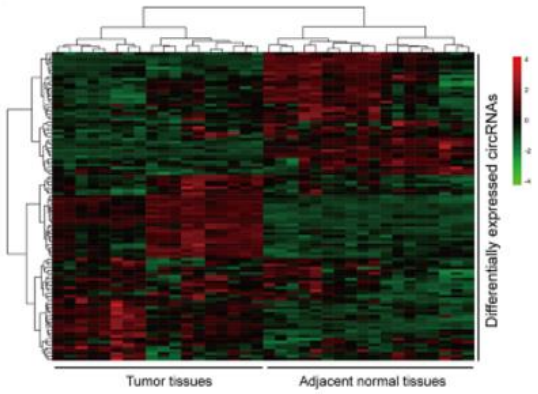
Differentially expressed circRNAs
Tumor tissues
Adjacent normal tissues

b)

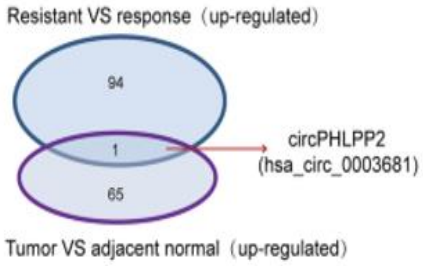
Resistant VS response (up-regulated)
94
1
65
circPHLPP2
(hsa_circ_0003681)
Tumor VS adjacent normal (up-regulated)

c)

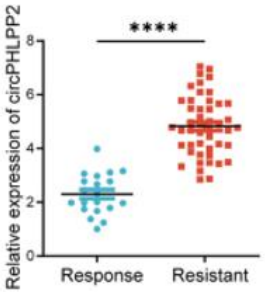
****
Relative expression of circPHLPP2
Response
Resistant

d)

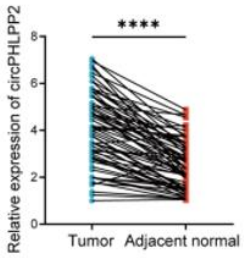
****
Relative expression of circPHLPP2
Tumor
Adjacent normal

e)

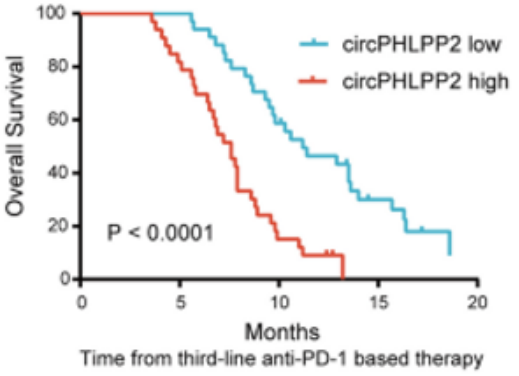
circPHLPP2 low
circPHLPP2 high
Overall Survival
P < 0.0001
Months
Time from third-line anti-PD-1 based therapy

f)

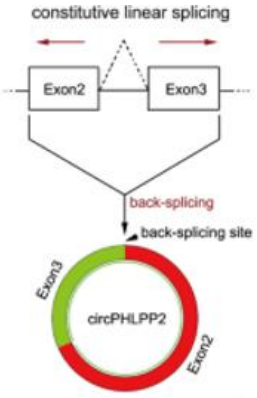
constitutive linear splicing
Exon2
Exon3
back-splicing
back-splicing site
Exon3
circPHLPP2
Exon2

g)

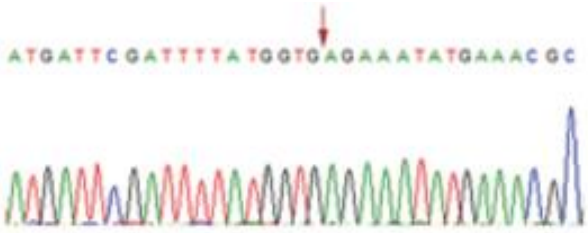
ATGATTCGATTTTATGGTGAGAAATATGAAACGC

h)

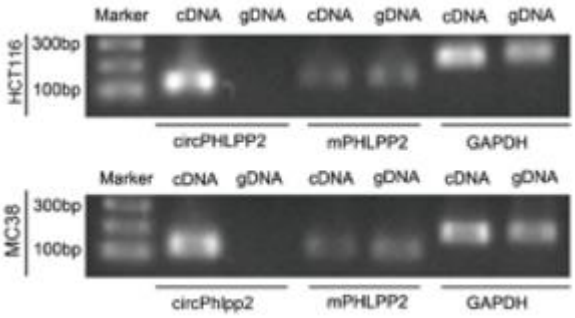
Marker
cDNA
gDNA
HCT116
300bp
100bp
circPHLPP2
mPHLPP2
GAPDH
MC38
circPhlpp2

i)

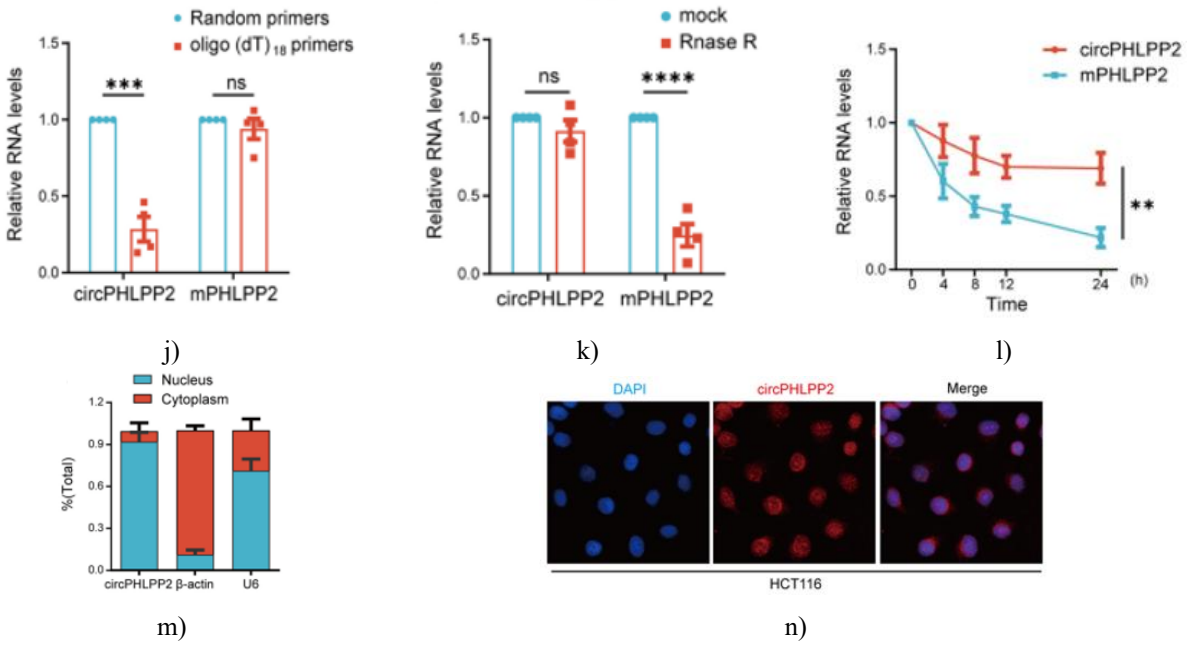

Figure 1. Patterns of circRNA expression in microsatellite stable/proficient mismatch repair (MSS/pMMR) colorectal cancer (CRC) and in-depth validation of circPHLPP2.

a Cluster analysis heatmap illustrating differential circRNA levels in MSS/pMMR CRC tumors from patients resistant (n=10) or sensitive (n=8) to anti-PD-1 treatment. **b** Cluster analysis heatmap comparing circRNA levels in MSS/pMMR CRC tumors (n=18) versus matched non-cancerous adjacent tissues (n=18), applying thresholds of Log_2(fold change) >1 or <−1 and P<0.05. **c** Venn diagram showing common upregulated circRNAs in anti-PD-1-resistant tumors and in CRC tumors compared to normal tissues. **d** RT-qPCR results showing higher circPHLPP2 levels in anti-PD-1-resistant (n=20) versus sensitive (n=47) tumor specimens. **e** RT-qPCR data revealing elevated circPHLPP2 in primary CRC tumors relative to paired normal adjacent tissues (n=67). **f** Kaplan–Meier curves demonstrating poorer overall survival in CRC patients with high circPHLPP2 expression (n=67, log-rank test). **g** Diagram outlining the back-splicing mechanism forming circPHLPP2. **h** Sanger sequencing verification of the circPHLPP2 back-splice junction. **i** RT-qPCR and gel electrophoresis confirming circPHLPP2 detection in HCT116 and MC38 cells. **j** Differential amplification of circPHLPP2 versus linear PHLPP2 mRNA using random hexamer versus oligo(dT)$_{18}$ primers in reverse transcription. **k** RT-qPCR assessment of circPHLPP2 and linear PHLPP2 resistance to RNase R exonuclease treatment. **l** RT-qPCR evaluation of circPHLPP2 and PHLPP2 mRNA stability after Actinomycin D (2 μg/ml) exposure. **m** Subcellular distribution of circPHLPP2 determined by nuclear/cytoplasmic RNA separation assay. **n** Fluorescence in situ hybridization (FISH) visualizing circPHLPP2 primarily in the nucleus of HCT116 cells (DAPI nuclear stain).

Statistics: Student's t-test applied to panels **d**, **e**, **j**, **k**; two-way ANOVA for **l**. Significance: **P<0.01, ***P<0.001, ****P<0.0001.

Biological features of circPHLPP2 in CRC cell models

Per the circBase database, circPHLPP2 arises from back-splicing of exons 2 and 3 in the PHLPP2 gene on chromosome 16 (positions 71736500–71748704), yielding a 424-nucleotide transcript **(Figure 1g).** Divergent primer amplification followed by Sanger sequencing validated the unique junction **(Figure 1h).** In HCT116 and MC38 cells, divergent primers detected circPHLPP2 only in cDNA (not gDNA), while convergent primers amplified linear PHLPP2 from both **(Figure 1i)**. Random primers enabled circPHLPP2 detection, unlike poly(A)-targeting oligo(dT)$_{18}$ primers **(Figure 1j),** confirming no poly-A tail. circPHLPP2 exhibited marked resistance to RNase R compared to linear PHLPP2 **(Figure 1k).** Transcription inhibition with Actinomycin D highlighted superior stability of circPHLPP2 **(Figure 1l),** consistent with its covalent

circular architecture. Both fractionation assays and FISH confirmed predominant nuclear retention **(Figures 1m-n).** These collective data authenticate circPHLPP2 as a true circular RNA molecule.

In vivo evidence for circPHLPP2 driving CRC tumor advancement

Overexpression constructs and back-splice-specific siRNAs effectively modulated circPHLPP2 levels in CRC cells **(Figures 1a-b).** In vitro assays (MTS proliferation and colony formation) showed no effect of altered circPHLPP2 on human CRC cell growth or clonogenicity **(Figures 2a-f).**

For in vivo studies, stable circPHLPP2-modified human CRC cells **(Figuers 1c-d)** were subcutaneously implanted into severely immunodeficient NSG mice, which lack T, B, and NK cells and antibody production [24]. No differences in tumor growth were observed **(Figures 2g, 2a and 2c).**

In contrast, implantation into BALB/c nude mice (T-cell deficient due to Foxn1 mutation but retaining B cells and potent NK activity [25]) revealed accelerated tumor expansion with circPHLPP2 **overexpression (Figures 2h and 2b)** and retardation with knockdown **(Figure 2d).** This implicated immune elements, likely NK or B cells, in circPHLPP2-mediated effects.

Similar pro-tumorigenic effects occurred upon overexpressing circPhlpp2 in MC38 (MSI-high CRC) cells implanted into immunocompetent C57BL/6 mice (**Figures 2i and 2e**; stable lines in **Figure 1e**). In the CT26 (MSS CRC) model [26], overexpression trended toward faster growth, achieving significance in terminal tumor mass **(Figures 2j and 2f).** Knockdown of circPhlpp2 in MC38 or CT26 cells **(Figure 1f)** robustly curtailed tumor expansion **(Figures 2g-h)** and improved survival in hosts **(Figures 2k-l).**

These findings collectively demonstrate that circPHLPP2 fosters CRC progression predominantly via alterations in the tumor-immune interface.

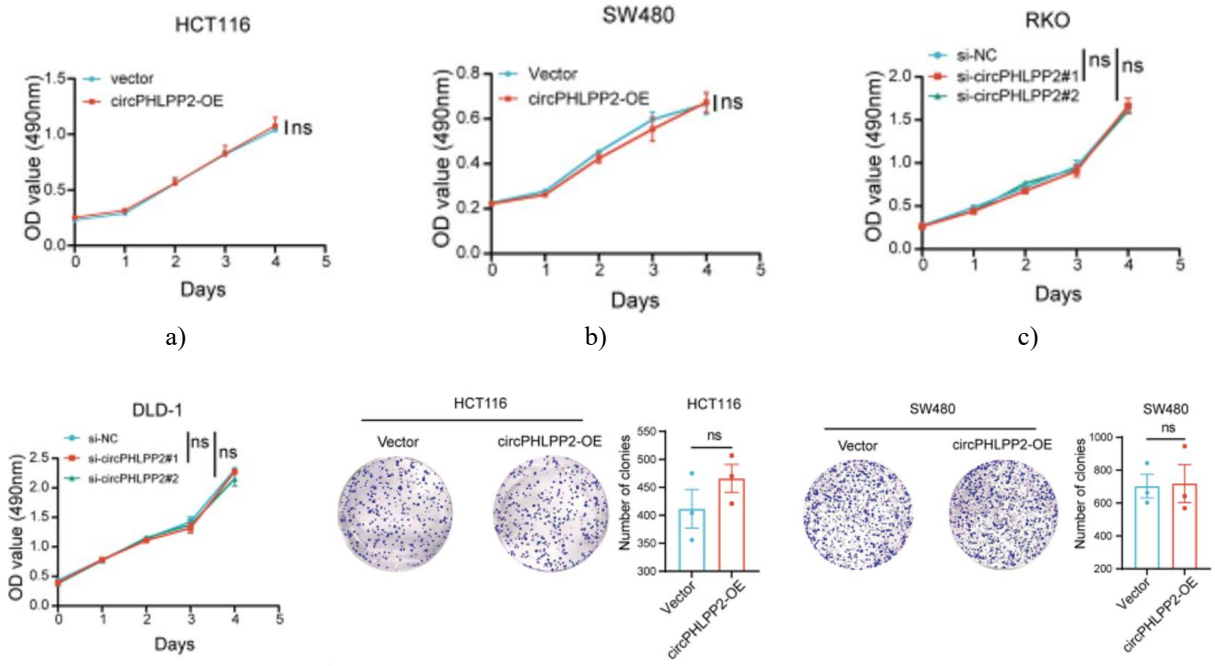

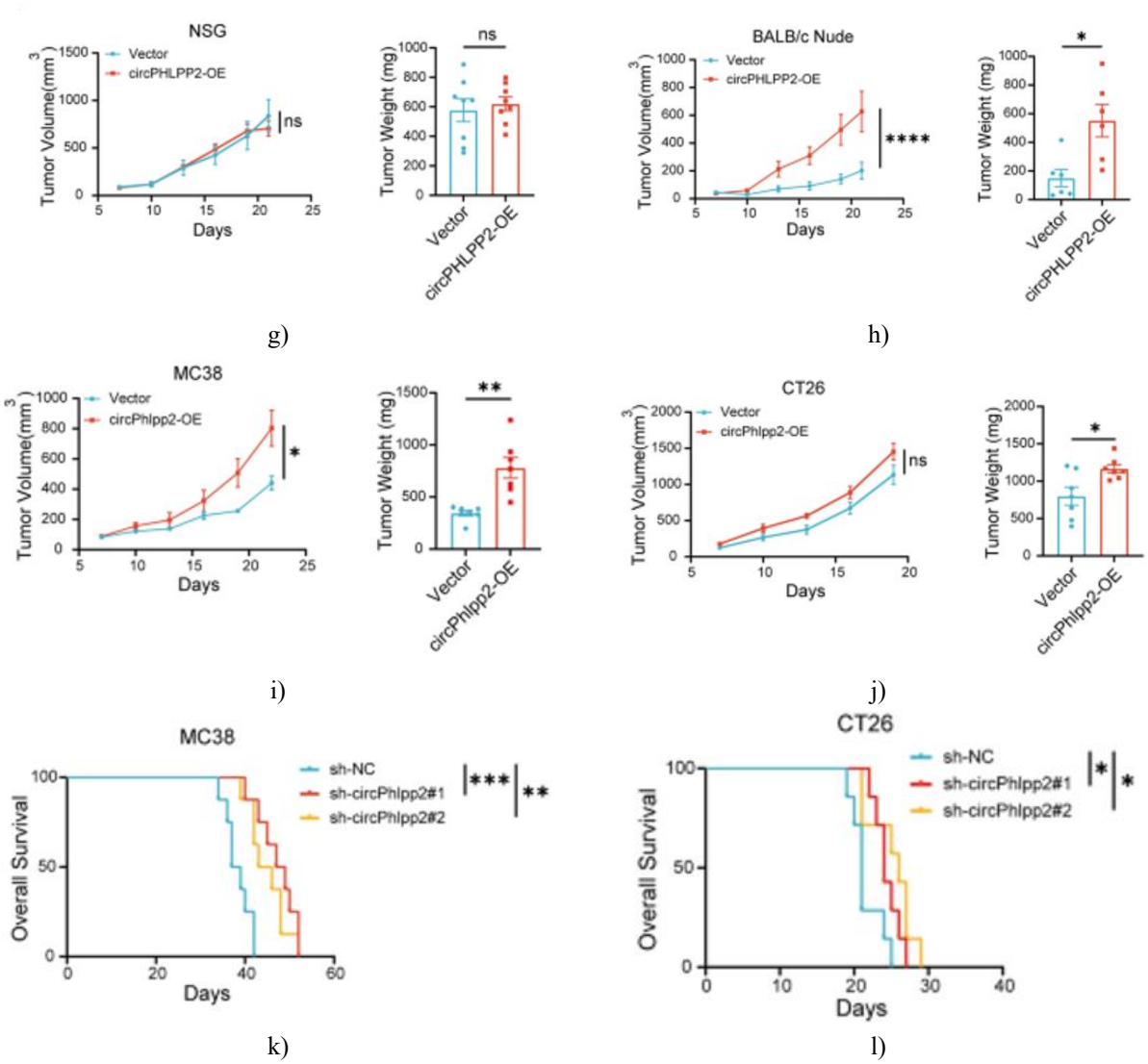

Figure 2. CircPHLPP2 enhances colorectal cancer (CRC) cell proliferation in vivo.

a-d In vitro proliferation of CRC cells with circPHLPP2 overexpression or knockdown, assessed via MTS assay. **e-f** Colony formation capacity of CRC cells following circPHLPP2 overexpression. **g** Tumor volume and weight in NSG mice subcutaneously implanted with HCT116 cells stably overexpressing circPHLPP2 (n = 8). **h** Tumor volume and weight in BALB/c nude mice subcutaneously implanted with HCT116 cells stably overexpressing circPHLPP2 (n = 6). **i** Tumor volume and weight in C57BL/6 mice subcutaneously implanted with MC38 cells stably overexpressing circPhlpp2 (n = 7). **j** Tumor volume and weight in BALB/c mice subcutaneously implanted with CT26 cells stably overexpressing circPhlpp2 (n = 7). **k-l** Kaplan–Meier survival curves for mice bearing MC38 tumors (n = 8) or CT26 tumors (n = 7) (log-rank test).

Statistical tests: two-way ANOVA for data in **a-d** and left panels of **g-j**; Student's t-test for **e-f** and right panels of **g-j**. Significance: *P < 0.05, **P < 0.01, ***P < 0.001, ****P < 0.0001.

CircPHLPP2 facilitates tumor progression through suppression of NK cell infiltration and reduction of granzyme B and IFN-γ production by NK cells

To investigate how circPHLPP2 affects immune cell composition within tumors, harvested tumors underwent multicolor flow cytometry. Results demonstrated that circPhlpp2 knockdown in both MC38 and CT26 models substantially increased the percentage of tumor-

infiltrating NK cells **(Figures 3a-b).** In MC38 tumors, circPhlpp2 knockdown also altered B cell proportions, an effect absent in CT26 tumors **(Figure 3c).** No notable changes were detected in other immune subsets **(Figures 4a-b),** pointing to a specific influence of circPhlpp2 on NK cell recruitment.

As key players in innate anti-tumor immunity, NK cells provide early defense against malignancy. Additional flow cytometry revealed that circPhlpp2 knockdown elevated NK cell frequencies not only within tumors but also in peripheral blood **(Figure 3d).** This indicates a broader systemic effect, whereby circPhlpp2 restricts NK cell availability in circulation, thereby limiting their infiltration into the tumor microenvironment (TME). Immunohistochemistry (IHC) further confirmed enhanced NK cell presence in tumors following circPhlpp2 knockdown **(Figure 3e).** Moreover, knockdown increased production of the cytotoxic effectors granzyme B and IFN-γ by tumor-infiltrating NK cells **(Figures 3f-g),** showing that circPhlpp2 dampens NK cell cytotoxic function.

To determine whether the pro-tumorigenic effects of circPhlpp2 depend on NK cells, NK depletion was performed prior to tumor implantation using anti-Asialo-GM1 or anti-NK1.1 antibodies **(Figure 4c).** NK cell depletion largely abrogated the growth inhibition caused by circPhlpp2 knockdown **(Figures 3h and 4d).** The partial rescue observed in MC38 models suggests additional NK-independent mechanisms may also contribute to circPhlpp2-driven tumor promotion **(Figure 3h).**

Overall, in both MSI-H and MSS CRC models, circPhlpp2 promotes immune escape by limiting NK cell infiltration and impairing their production of cytotoxic cytokines, thereby supporting tumor expansion. In contrast, reducing circPhlpp2 levels boosts NK cell tumor infiltration and enhances granzyme B and IFN-γ expression, strengthening anti-tumor immunity.

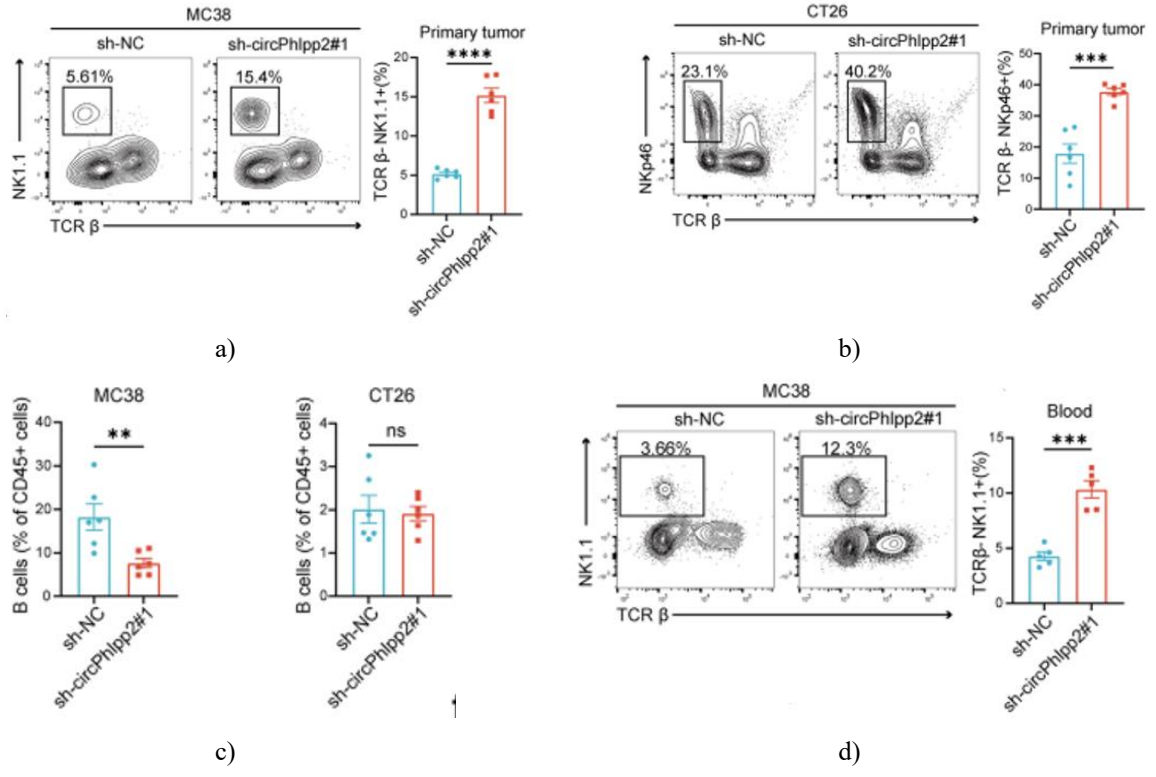

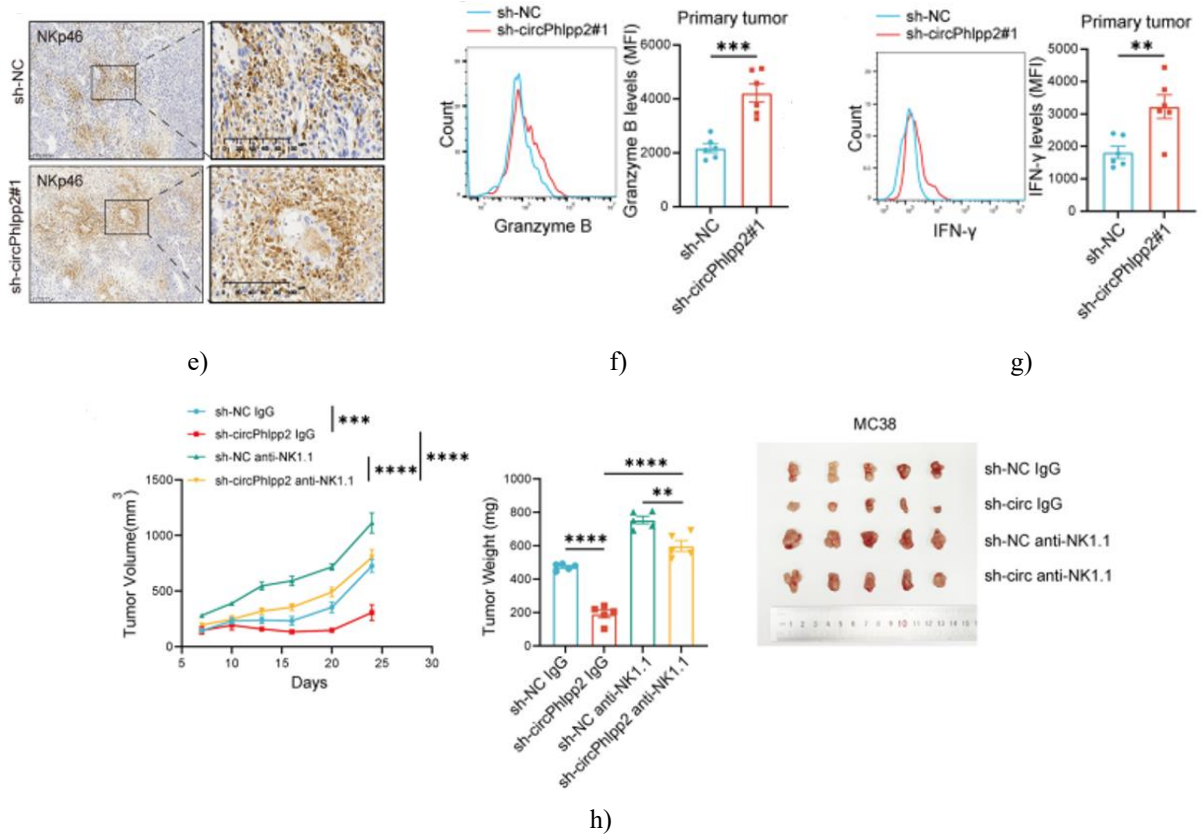

Figure 3. CircPHLPP2 diminishes NK cell frequency and lowers granzyme B plus IFN-γ levels in NK cells.

a-b Flow cytometry results for NK cells in tumors grown in C57BL/6 mice (**a**) or BALB/c mice (**b**): example gating plots (left) and pooled percentage data (right) for control versus circPhlpp2-depleted tumors (n=6). **c** Proportion of B cells detected by flow cytometry in tumors from C57BL/6 mice (left) or BALB/c mice (right) with or without circPhlpp2 depletion (n=6). **d** Analysis of circulating NK cells in blood from tumor-bearing C57BL/6 mice: typical flow plots (left) and compiled quantification (right) comparing knockdown and control conditions (n=5). **e** Typical immunohistochemistry images showing NKp46-positive NK cells in C57BL/6 mouse tumors with or without circPhlpp2 knockdown; scale bar represents 400 μm. **f-g** Levels of granzyme B (**f**) and IFN-γ (**g**) produced by tumor-resident NK cells from C57BL/6 mice, with or without circPhlpp2 knockdown (n=6). **i** Tumor growth trajectories, endpoint masses, and photographic examples of syngeneic grafts in C57BL/6 mice with or without NK cell depletion (n=5) (left panel: two-way ANOVA; middle panel: one-way ANOVA).

Statistics applied: Student's t-test for panels **a-d** and **f-g**. Significance indicated as **P<0.01, ***P<0.001, ****P<0.0001.

IL36γ serves as an important effector molecule downstream of circPHLPP2

To identify genes regulated by circPHLPP2, transcriptome profiling via RNA sequencing was carried out in HCT116 cells transduced with either circPHLPP2-overexpressing or control lentivirus. Enrichment analysis using KEGG pathways highlighted significant engagement of circPHLPP2 in cytokine–cytokine receptor signaling **(Figure 4a).** Key genes showing differential expression—such as IL36γ, CCL5, IFNE, and GDF7—mapped predominantly to this pathway **(Figure 4b).**

Mining of TCGA colorectal cancer cohorts (COAD and READ) uncovered a strong inverse relationship between IL36γ levels and estimated NK cell abundance (**Figure 5a)**, positioning IL36γ as a plausible mediator for circPHLPP2's effects. Since cytokines can profoundly influence the tumor milieu, expression of candidate

cytokines (IL36γ, CCL5, IFNE, GDF7) was assessed by RT-qPCR in stable circPHLPP2-overexpressing HCT116 and SW480 lines versus controls. Of these, IL36γ emerged as the only cytokine reliably induced across both cell types **(Figure 4c).**

Protein analysis by western blot showed that raising circPHLPP2 boosted IL36γ abundance, while lowering it had the reverse effect in human colorectal cancer lines (**Figures 4d-e**). Parallel observations of increased IL36γ protein upon circPhlpp2 modulation were made in mouse-derived CRC cells (**Figure 5b**). Altogether, these data support a model in which circPHLPP2 drives upregulation of IL36γ at both mRNA and protein stages.

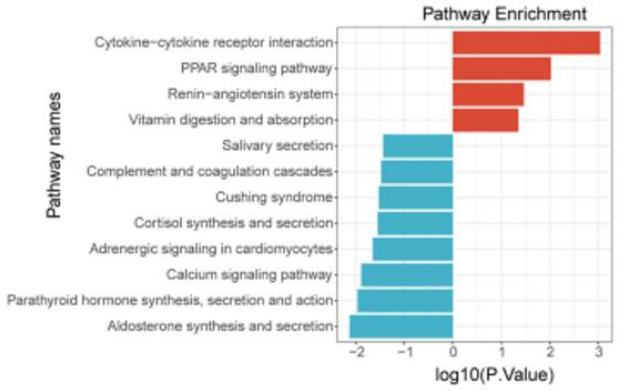

a)

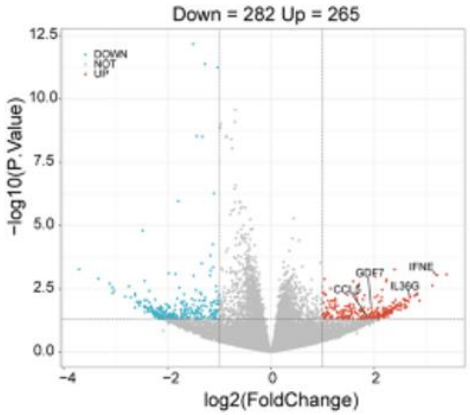

b)

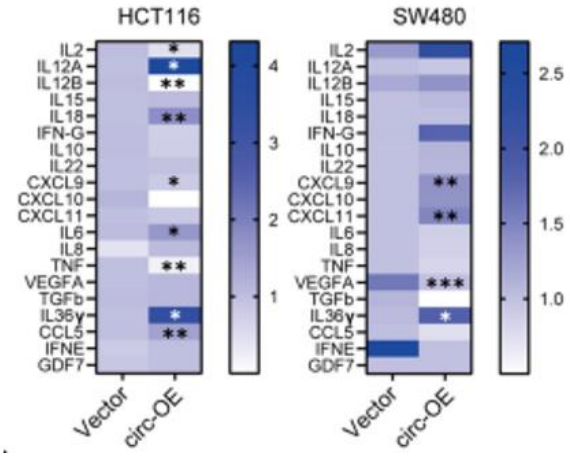

c)

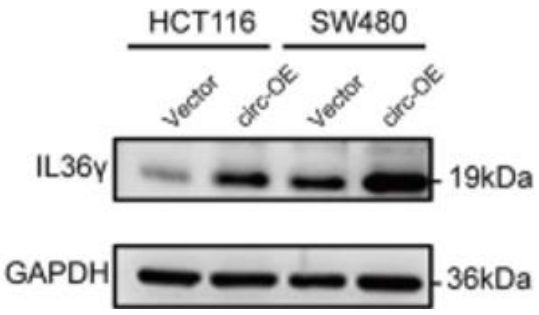

d)

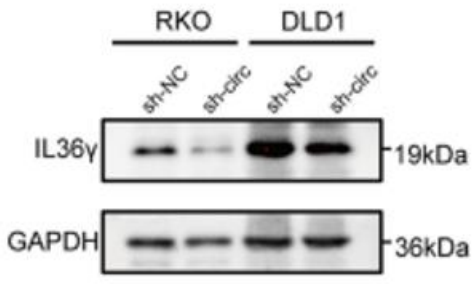

e)

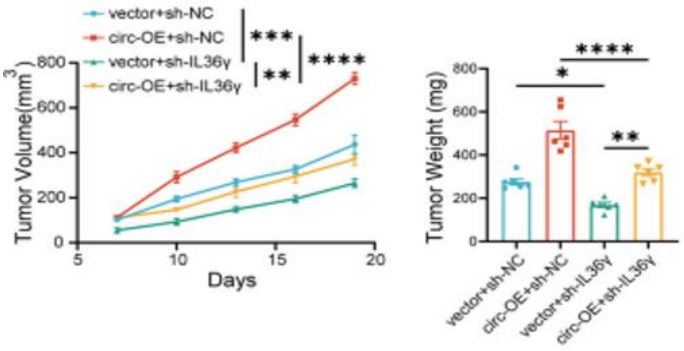

f)

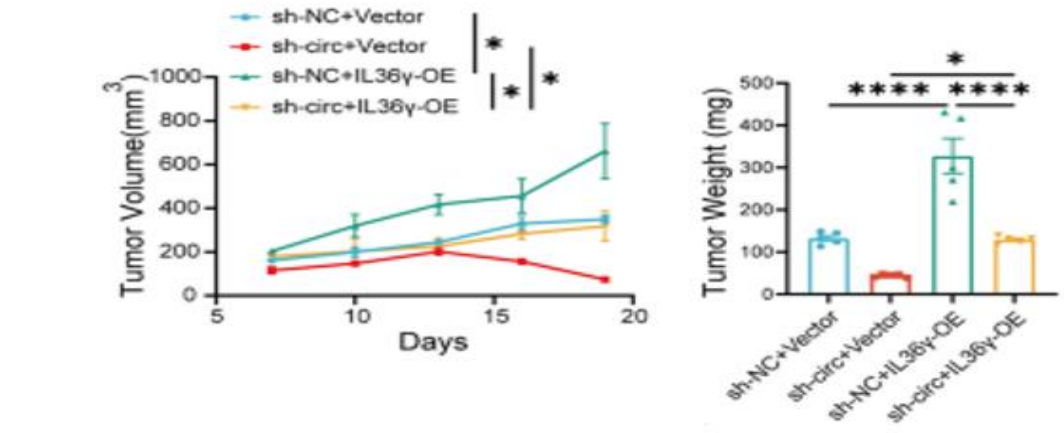

g)

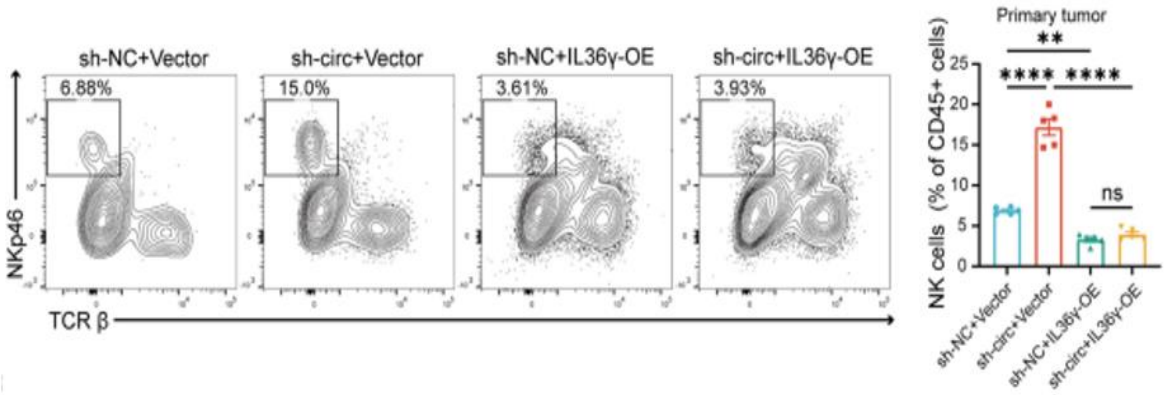

h)

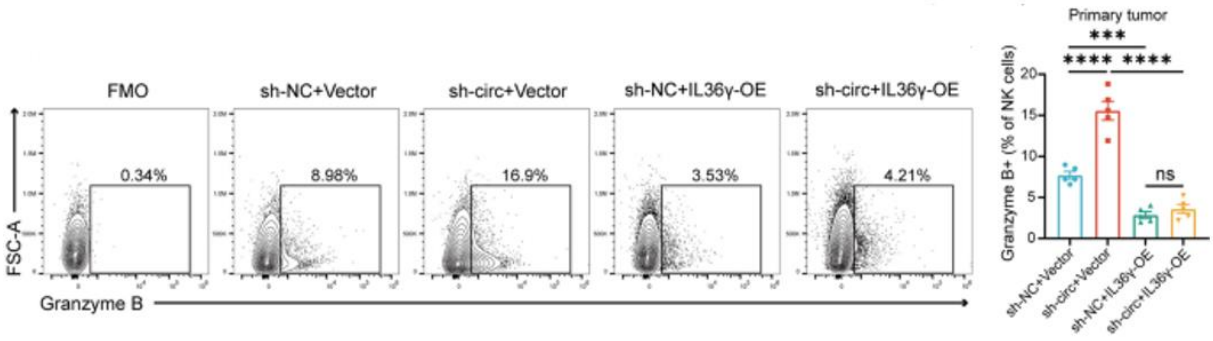

i)

Figure 4. IL36γ functions as a key downstream target of circPHLPP2.

a KEGG pathway enrichment results for differentially expressed mRNAs. Differentially expressed genes (DEGs) were determined using the limma R package with criteria of $|\log_2(\text{fold change})| > 1$ and $P < 0.05$. **b** Volcano plot displaying up- and down-regulated genes; genes belonging to the cytokine–cytokine receptor interaction pathway are highlighted. **c** Heatmap illustrating relative mRNA levels of selected cytokines, measured by RT-qPCR, in HCT116 and SW480 cells transduced with circPHLPP2 overexpression or control vector lentivirus (data normalized to vector control). **d-e** Western blot analysis of IL36γ protein in human CRC cells following circPHLPP2 overexpression (**d**) or knockdown (**e**). **f** Tumor growth curves (left) and final

tumor weights (right) of syngeneic allografts in C57BL/6 mice implanted with MC38 cells modified for circPhlpp2 overexpression alone or combined with IL36γ knockdown (n=5). **g** Tumor growth curves (left) and final tumor weights (right) in C57BL/6 mice implanted with MC38 cells modified for circPhlpp2 knockdown alone or combined with IL36γ overexpression (n=5). **h** Flow cytometry analysis of NK cell frequency in tumors: representative plots (left) and quantification (right) for circPhlpp2 knockdown alone or with IL36γ overexpression in C57BL/6 mice (n=5). **i** Granzyme B expression in tumor-infiltrating NK cells under circPhlpp2 knockdown alone or combined with IL36γ overexpression, assessed by flow cytometry (n=5).

Statistical tests: two-way ANOVA for growth curves in **f-g** (left); one-way ANOVA for endpoint data in **f-i** (right). Significance: *P<0.05, **P<0.01, ***P<0.001, ****P<0.0001.

Previous studies have documented elevated IL36γ expression in colorectal cancer tissues and its correlation with poorer patient outcomes. IL36γ is also known to drive production of multiple inflammatory factors that critically shape the tumor immune microenvironment [27]. Consistent with these reports, our analysis revealed that high IL36γ levels correlated with reduced overall survival in CRC patients **(Figures 5c-d).** Moreover, IL36γ overexpression accelerated MC38 tumor growth in vivo **(Figure 5e)** and decreased NK cell infiltration into the tumor bed **(Figure 5f).** Thus, IL36γ mirrors the tumor-promoting phenotype observed with circPHLPP2. To test whether IL36γ mediates circPHLPP2's effects, rescue experiments were performed. Knocking down IL36γ markedly reversed the enhanced tumor growth induced by circPhlpp2 overexpression **(Figures 4f and 6c).** Conversely, forced IL36γ expression largely restored tumor proliferation, reduced NK cell abundance, and lowered granzyme B and IFN-γ levels that had been altered by circPhlpp2 knockdown in MC38 cells **(Figures 4g-I and 6d-f).** These findings demonstrate that circPHLPP2 promotes CRC progression primarily through upregulation of IL36γ.

CircPHLPP2 enhances IL36γ transcription via interaction with ILF3

To elucidate the mechanism by which circPHLPP2 regulates IL36γ expression, potential modes of action were examined. The CircInteractome database predicts numerous miRNA-binding sites on circPHLPP2 but no association with AGO2, the core component that directs miRNAs to target mRNAs [28]. This led to the hypothesis that circPHLPP2 acts through protein interactions.

MS2-tagged RNA pull-down assays were employed to identify circPHLPP2-binding proteins. Successful enrichment of the bait protein MCP-GST **(Figure 7a)** and high recovery of circPHLPP2 **(Figure 7b)** confirmed assay specificity. Mass spectrometry ranked HNRNPC highest; however, given its known broad role in circRNA biogenesis rather than specific functional binding, focus shifted to lower-ranked candidates. FISH assays tested the second-ranked ILF3 and third-ranked PABPC1. ILF3 showed clear colocalization with circPHLPP2, and circPHLPP2 overexpression increased nuclear ILF3 signal **(Figure 5a).** Co-transfection of MS2-tagged circPHLPP2 with MCP-GST strongly enriched ILF3 relative to control **(Figure 5b),** and RNA immunoprecipitation (RIP) with anti-ILF3 antibody specifically pulled down circPHLPP2 in CRC cells **(Figure 5c).** These results establish a direct interaction between circPHLPP2 and ILF3. The ILF3 peptide spectrum from mass spectrometry is presented in **Figure 5d**. Subcellular fractionation further confirmed elevated nuclear ILF3 protein upon circPHLPP2 overexpression **(Figure 5e).**

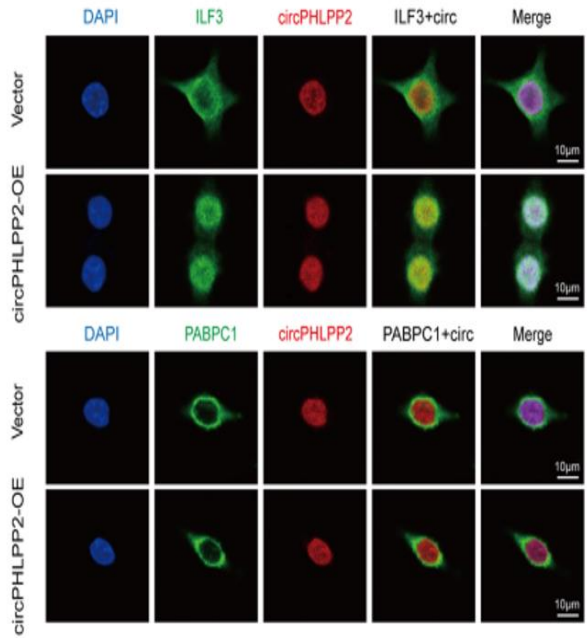
DAPI
ILF3
circPHLPP2
ILF3+circ
Merge
Vector
circPHLPP2-OE
10μm
DAPI
PABPC1
circPHLPP2
PABPC1+circ
Merge
Vector
circPHLPP2-OE
10μm

a)

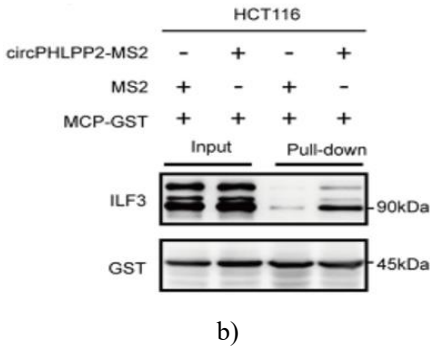
HCT116
circPHLPP2-MS2 - + - +
MS2 + - + -
MCP-GST + + + +
Input
Pull-down
ILF3
90kDa
GST
45kDa

b)

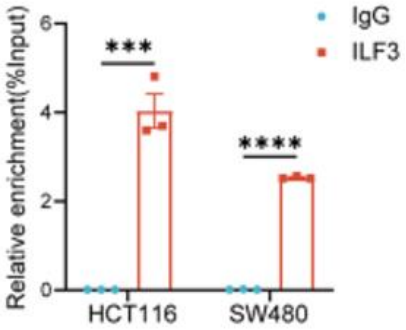
IgG
ILF3
Relative enrichment(%Input)
6
4
2
0
***
****
HCT116
SW480

c)

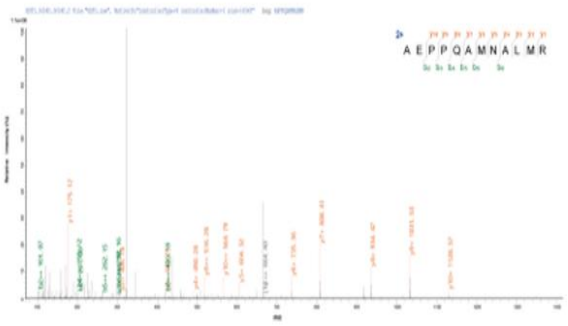
A E P P Q A M N A L M R

d)

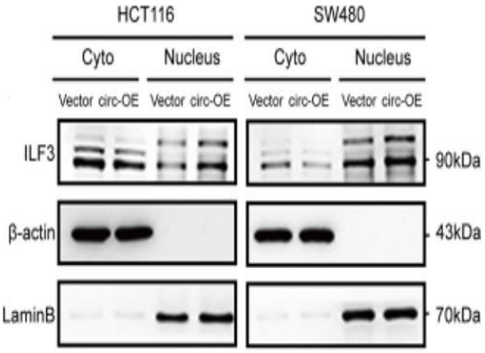
HCT116
SW480
Cyto
Nucleus
Cyto
Nucleus
Vector circ-OE Vector circ-OE Vector circ-OE Vector circ-OE
ILF3
90kDa
β-actin
43kDa
LaminB
70kDa

e)

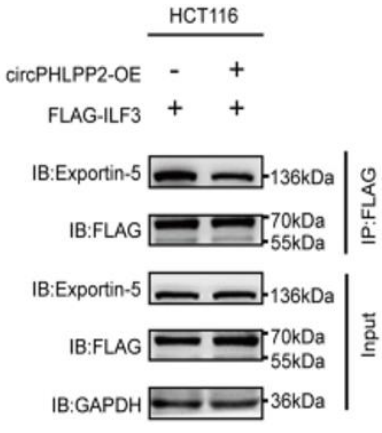
HCT116
circPHLPP2-OE - +
FLAG-ILF3 + +
IB:Exportin-5
136kDa
IB:FLAG
70kDa
55kDa
IP:FLAG
IB:Exportin-5
136kDa
IB:FLAG
70kDa
55kDa
Input
IB:GAPDH
36kDa

f)

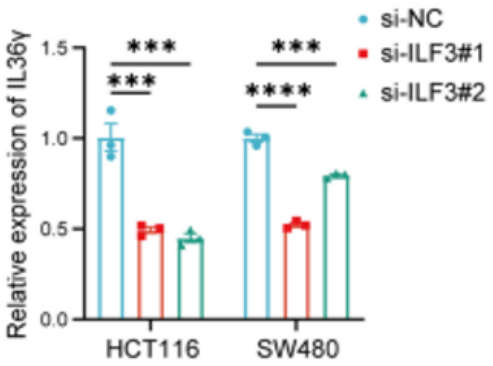
si-NC
si-ILF3#1
si-ILF3#2
Relative expression of IL36γ
1.5
1.0
0.5
0.0
***
***
***
****
HCT116
SW480

g)

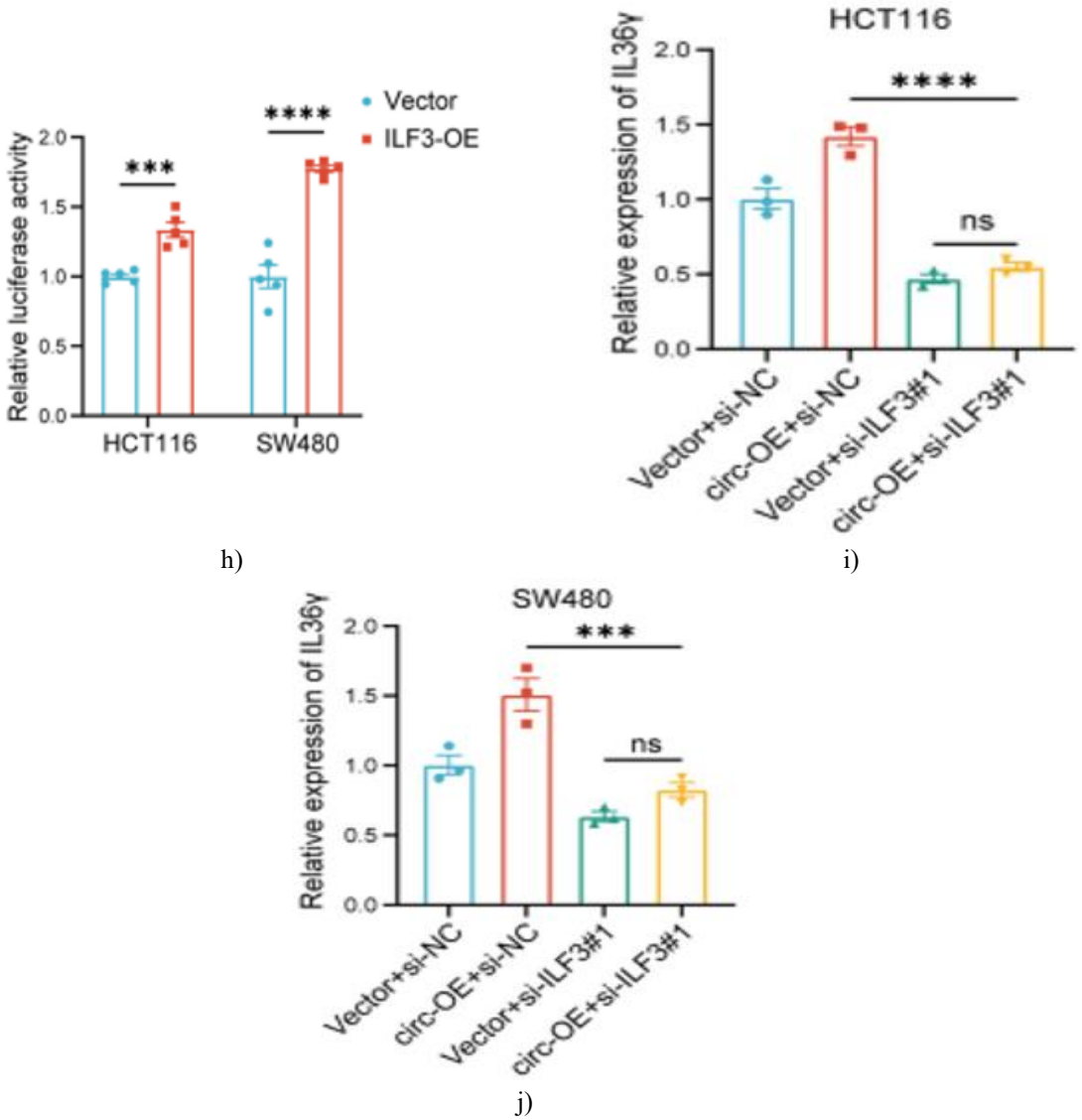

Figure 5. CircPHLPP2 promotes IL36γ transcription through direct interaction with ILF3.

a Combined RNA-FISH (for circPHLPP2) and immunofluorescence (for ILF3 or PABPC1) showing colocalization in HCT116 cells; scale bar = 10 μm. **b** MS2-based RNA pull-down assay demonstrating specific binding of ILF3 to circPHLPP2. **c** RNA immunoprecipitation (RIP) using anti-ILF3 antibody or IgG control in HCT116 and SW480 cells, followed by RT-qPCR to quantify enriched circPHLPP2. **d** Mass spectrometry identification of ILF3 as a circPHLPP2-interacting protein. **e** Western blot detection of ILF3 protein in cytoplasmic and nuclear fractions of HCT116 and SW480 cells with or without circPHLPP2 overexpression. **f** Co-immunoprecipitation (Co-IP) followed by western blotting to assess ILF3 interaction with exportin-5 in control versus circPHLPP2-overexpressing HCT116 cells. **g** RT-qPCR measurement of IL36γ mRNA in HCT116 and SW480 cells after transfection with two independent ILF3-targeting siRNAs (si-ILF3#1, si-ILF3#2) or negative control siRNA. **h** Luciferase reporter assay (firefly/renilla ratio) in HCT116 and SW480 cells co-transfected with an IL36γ promoter-driven luciferase construct and either ILF3 overexpression plasmid or empty vector. **i-j** RT-qPCR analysis of IL36γ mRNA levels in HCT116 (**i**) and SW480 (**j**) cells subjected to circPHLPP2 overexpression alone or combined with ILF3 knockdown.

Statistical tests: Student's t-test for data in **c** and **h**; one-way ANOVA for **g**, **i**, and **j**. Significance: ***$P < 0.001$, ****$P < 0.0001$.

ILF3 (also referred to as NF90/NF110) is a double-stranded RNA-binding protein that forms complexes with various proteins, mRNAs, small non-coding RNAs, and dsRNAs to control gene expression and mRNA stability [29]. Its functional roles are closely linked to subcellular localization [30]. As a nucleocytoplasmic shuttling protein, ILF3 export to the cytoplasm relies on exportin-5, which fails to transport ILF3 when it is bound to RNA [31]. Prior work has shown that circRNA–ILF3 complexes can alter ILF3 localization and modulate host immune responses [32]. We therefore hypothesized that circPHLPP2 binds ILF3 competitively, reducing its association with exportin-5 and leading to nuclear retention of ILF3. Co-IP experiments confirmed that circPHLPP2 overexpression disrupted the ILF3–exportin-5 interaction, supporting this model (**Figure 5f**). ILF3 contains a nuclear localization signal, two dsRNA-binding domains (dsRBDs), an RGG motif, and a glycine/arginine-rich C-terminal region [33]. Exportin-5 binds the dsRBDs of ILF3, and dsRNA occupancy of this region blocks exportin-5 binding [31]. We posited that circPHLPP2 engages the dsRBDs, thereby preventing exportin-5 interaction. GST pull-down assays demonstrated loss of circPHLPP2 binding to a dsRBD-deleted ILF3 mutant (ILF3 △d), validating this mechanism **(Figure 7c).**

Given the nuclear colocalization of circPHLPP2 and ILF3, we investigated whether ILF3 directly controls IL36γ transcription. Two independent siRNAs efficiently reduced ILF3 mRNA **(Figure 7d)** and consequently lowered IL36γ expression in CRC cells **(Figure 5g)**. An IL36γ promoter luciferase reporter assay revealed that ILF3 overexpression significantly enhanced luciferase activity **(Figure 5h),** confirming ILF3 as a positive transcriptional regulator of IL36γ. Importantly, ILF3 depletion largely abolished the IL36γ induction triggered by circPHLPP2 overexpression **(Figures 5i-j),** establishing that circPHLPP2-driven IL36γ upregulation requires ILF3. These collective findings indicate that circPHLPP2 boosts IL36γ transcription via physical association with ILF3.

Depletion of circPhlpp2 improves anti-PD-1 therapeutic response in vivo

Our data established that circPhlpp2 drives CRC growth in vivo, suppresses NK cell activity, and dampens antitumor immunity. We next examined whether targeting circPhlpp2 could enhance anti-PD-1 immunotherapy. Tumor progression was monitored in immunocompetent mouse models treated with circPhlpp2 knockdown, anti-PD-1 antibody, or both.

In the MC38 model (MSI-H CRC, highly immunotherapy-sensitive [34]), anti-PD-1 monotherapy slowed tumor growth, but circPhlpp2 knockdown alone achieved stronger inhibition **(Figures 6a-c).** In the CT26 model (MSS CRC, typically immunotherapy-resistant [35]), anti-PD-1 had minimal effect, whereas circPhlpp2 knockdown showed a modest suppressive trend **(Figures 6d-f)**. Notably, combining anti-PD-1 with circPhlpp2 knockdown yielded superior tumor control compared to anti-PD-1 alone in both models, particularly evident in tumor volume reduction **(Figures 6a and 6d).** These results demonstrate that circPhlpp2 depletion substantially sensitizes tumors to PD-1 blockade, augmenting anti-PD-1 efficacy.

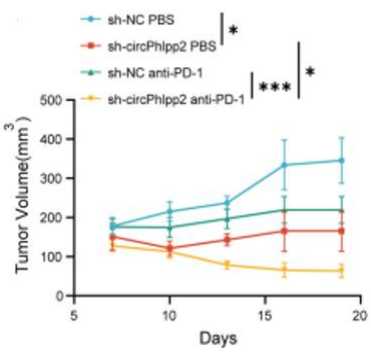

a)

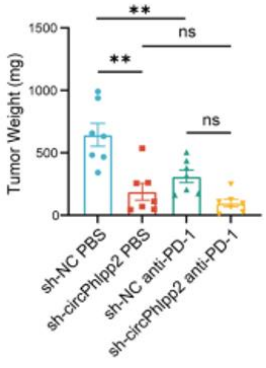

b)

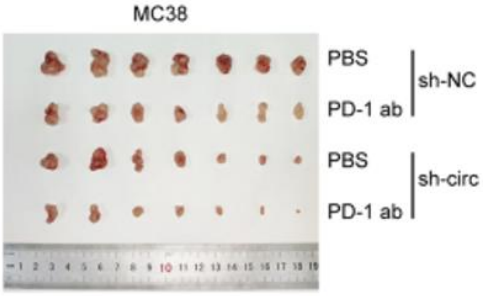

c)

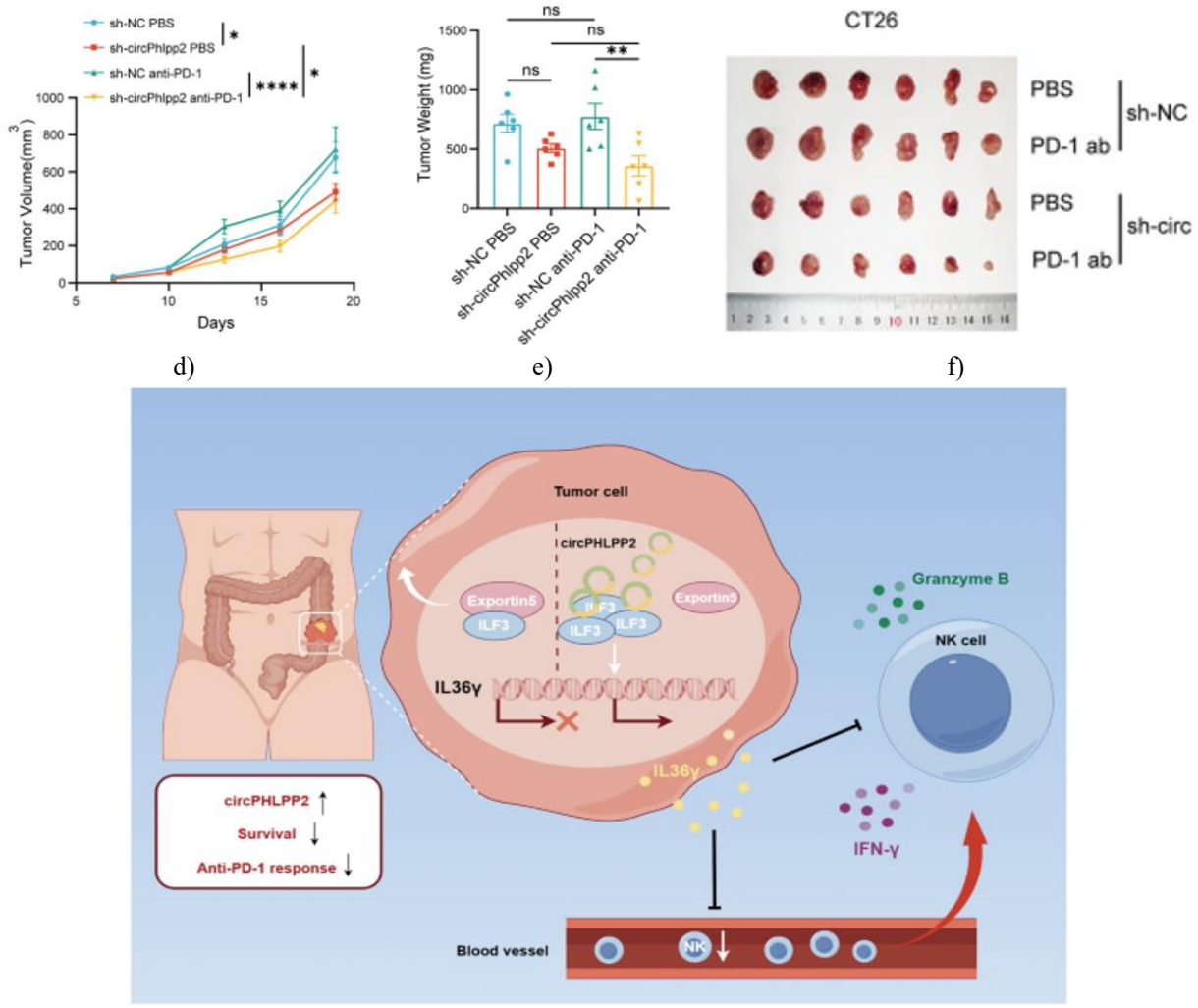

Figure 6. Silencing of circPHLPP2 improves the effectiveness of anti-PD-1 immunotherapy in animal models.

a-c Tumor growth curves (volume) (a) and final tumor weights (b) from subcutaneous allografts in C57BL/6 mice implanted with MC38 cells, either control or with circPhlpp2 knockdown. Following anti-PD-1 antibody administration, excised tumors were imaged (c) (n = 7 per group). **d-f** Tumor growth curves (volume) (d) and final tumor weights (e) from subcutaneous allografts in BALB/c mice implanted with CT26 cells, either control or with circPhlpp2 knockdown. Following anti-PD-1 antibody administration, excised tumors were imaged (f) (n = 6 per group). **g** Illustrative model showing how circPHLPP2 drives colorectal cancer (CRC) progression by binding to ILF3, thereby increasing IL36γ expression. This leads to decreased natural killer (NK) cell tumor infiltration and reduced granzyme B and IFN-γ production by NK cells. Inhibiting circPHLPP2 could potentially boost the therapeutic impact of anti-PD-1 treatment in CRC patients (created using Figdraw).

Statistical analysis: Data in panels **a** and **d** were evaluated using two-way ANOVA. Data in panels **b** and **e** were evaluated using one-way ANOVA. Significance levels: *P < 0.05, **P < 0.01, ***P < 0.001, ****P < 0.0001.

Cancer immunotherapy has recently demonstrated notable antitumor effects across various tumor types, including colorectal cancer (CRC). Nonetheless, immune therapy resistance remains a major challenge, particularly in CRC patients with MSS/pMMR status [36]. Emerging evidence indicates that circular RNAs (circRNAs) contribute to tumor progression [37], and some circRNAs have been linked to the response to anti-PD-1 therapy [38]. Investigating circRNAs that modulate the immune microenvironment may provide valuable

insights into predictive biomarkers for immunotherapy and identify potential therapeutic targets. In this study, we identified circPHLPP2 as being associated with anti-PD-1 responsiveness in MSS/pMMR advanced CRC patients and, for the first time, elucidated its functional mechanism in immune evasion. Furthermore, we proposed a strategy to potentially enhance anti-PD-1 therapy efficacy in CRC.

By analyzing circPHLPP2 expression in a cohort of CRC patients receiving anti-PD-1-based treatment, we found that circPHLPP2 levels were significantly higher in CRC tissues compared to adjacent normal tissues and were particularly elevated in patients resistant to anti-PD-1 therapy. Patients with high circPHLPP2 expression also exhibited poorer overall survival, suggesting that circPHLPP2 may act as a tumor-promoting factor. Subsequent functional studies revealed that circPHLPP2 did not affect CRC cell proliferation in vitro but promoted tumor growth in both nude and immunocompetent mice, indicating its involvement in tumor–immune cell interactions. Specifically, circPHLPP2 reduced NK cell abundance in peripheral blood and tumor infiltration, along with decreased granzyme B and IFN-γ expression, facilitating immune evasion. Considering NK cells' cytotoxic activity via ADCC and other mechanisms, further research is warranted to investigate circPHLPP2's broader effects on NK cell function. Although T cells are the primary mediators of checkpoint inhibitor efficacy, CTLA-4 or PD-1 blockade can also enhance NK cell-mediated antitumor responses [39]. Prior studies have shown that circUHRF1 drives anti-PD-1 resistance in HCC by impairing NK cell function [40]. Together, these findings suggest that circPHLPP2 contributes to anti-PD-1 resistance in MSS/pMMR advanced CRC by modulating NK cells, and its inhibition can improve therapy outcomes, making it a promising therapeutic target.

Previous research has demonstrated that circRNAs can regulate immune activation or tolerance by modulating cytokines and chemokines. For instance, circCYP24A1 can influence the tumor microenvironment through CCL5 secretion [41]. In this study, we found that circPHLPP2 participates in the cytokine–cytokine receptor interaction pathway, with IL36γ acting as a downstream effector. IL36γ has been implicated in tumor progression and metastasis in multiple cancers; for example, it promotes non-small cell lung cancer progression by enhancing GSH biogenesis and mitigating oxidative stress-induced cell death [42]. Additionally, IL36γ contributes to colon inflammation and tumorigenesis by modulating cell-matrix adhesion and Wnt signaling [27]. In CRC, high IL-36α and IL-36β levels, or high IL-36α combined with low IL-36γ, correlate with better survival, highlighting their prognostic potential. These studies support the pro-tumorigenic role of IL36γ, consistent with our observations. Notably, IL36γ's role in immune regulation is context-dependent: it enhances antitumor immunity in melanoma by boosting IFN-γ production in CD8+ T cells and NK cells [43], while in colitis, it inhibits Treg differentiation and promotes Th9 polarization [44]. Our data show that, similar to circPHLPP2, IL36γ promotes CRC cell proliferation and reduces NK cell infiltration and effector molecule expression, and IL36γ overexpression can rescue the effects of circPHLPP2 knockdown. These results suggest that circPHLPP2 contributes to CRC progression partly through IL36γ secretion, with the impact of IL36γ varying according to tissue and disease context.

CircRNAs can function as miRNA sponges, interact with RNA-binding proteins (RBPs), or potentially encode peptides, with their roles depending on subcellular localization [45]. Nuclear circRNAs, for instance, regulate transcription, alternative splicing, and chromatin looping [37]. In our study, FISH analysis revealed that circPHLPP2 is primarily nuclear and directly binds ILF3, promoting its nuclear accumulation. ILF3 nuclear export requires binding to exportin-5, which can be inhibited by RNA interactions [31]. We demonstrated that circPHLPP2 binding reduces ILF3–exportin-5 interaction, increasing nuclear ILF3 levels. ILF3 is known to influence cancer pathogenesis, progression, drug resistance, and prognosis [29, 46, 47] and can regulate transcription, translation, mRNA stability, and microRNA processing [48, 49]. Within the nucleus, ILF3 controls transcription of genes such as TGF-β2 and uPA [46, 50]. Our results show that ILF3 enhances IL36 transcription, and circPHLPP2 facilitates ILF3 nuclear accumulation, leading to elevated IL36γ expression.

This study has several limitations. First, the sample size is small, and validation in larger patient cohorts is needed. Second, the precise mechanisms by which IL36γ modulates NK cell infiltration and function remain unclear and require further investigation. Third, mouse models cannot fully recapitulate the human tumor immune microenvironment; thus, studies using humanized mouse models are warranted to confirm these findings.

Conclusion

In summary, circPHLPP2 drives CRC progression by reshaping the tumor microenvironment. Mechanistically, circPHLPP2 promotes CRC cell growth by upregulating IL36γ via its interaction with ILF3, which in turn diminishes NK cell infiltration and decreases NK cell granzyme B and IFN-γ expression **(Figure 6g).** Therefore, targeting circPHLPP2 could improve the therapeutic response to anti-PD-1 treatment in CRC patients.

Acknowledgments: We thank all the patients enrolled in this study.

Conflict of Interest: None

Financial Support: This research was supported by National Natural Science Foundation of China (No.82373376) and Natural Science Foundation of Guangdong Province (No. 2023A1515030257).

Ethics Statement: The study was approved by the Medical Ethics Committee of Sun Yat-sen University Cancer Center (SYSUCC) with written informed consents from all the patients (SZR2022-008). The animal studies were ethically approved by the Institutional Ethics Committee for Clinical Research and Animal Trials of the SYSUCC (L102022022003L).

References

1. Sung H, Ferlay J, Siegel RL, Laversanne M, Soerjomataram I, Jemal A, Bray F. Global Cancer statistics 2020: GLOBOCAN estimates of incidence and Mortality Worldwide for 36 cancers in 185 countries. CA Cancer J Clin. 2021;71:209–49.
2. Guo S, Sun Y. OTOP2, inversely modulated by miR-3148, inhibits CRC Cell Migration, Proliferation and epithelial-mesenchymal transition: evidence from Bioinformatics Data Mining and Experimental Verification. Cancer Manag Res. 2022;14:1371–84.
3. Diaz LA Jr., Shiu KK, Kim TW, Jensen BV, Jensen LH, Punt C, Smith D, Garcia-Carbonero R, Benavides M, Gibbs P, et al. Pembrolizumab versus chemotherapy for microsatellite instability-high or mismatch repair-deficient metastatic colorectal cancer (KEYNOTE-177): final analysis of a randomised, open-label, phase 3 study. Lancet Oncol. 2022;23:659–70.
4. Manca P, Corti F, Intini R, Mazzoli G, Miceli R, Germani MM, Bergamo F, Ambrosini M, Cristarella E, Cerantola R, et al. Tumour mutational burden as a biomarker in patients with mismatch repair deficient/microsatellite instability-high metastatic colorectal cancer treated with immune checkpoint inhibitors. Eur J Cancer. 2023;187:15–24.
5. He X, Xu C. Immune checkpoint signaling and cancer immunotherapy. Cell Res. 2020;30:660–9.
6. Fukuoka S, Hara H, Takahashi N, Kojima T, Kawazoe A, Asayama M, Yoshii T, Kotani D, Tamura H, Mikamoto Y, et al. Regorafenib Plus Nivolumab in patients with Advanced gastric or colorectal Cancer: an Open-Label, Dose-Escalation, and dose-expansion phase ib trial (REGONIVO, EPOC1603). J Clin Oncol. 2020;38:2053–61.
7. Zhou WY, Cai ZR, Liu J, Wang DS, Ju HQ, Xu RH. Circular RNA: metabolism, functions and interactions with proteins. Mol Cancer. 2020;19:172.
8. Long F, Lin Z, Li L, Ma M, Lu Z, Jing L, Li X, Lin C. Comprehensive landscape and future perspectives of circular RNAs in colorectal cancer. Mol Cancer. 2021;20:26.
9. Ju HQ, Zhao Q, Wang F, Lan P, Wang Z, Zuo ZX, Wu QN, Fan XJ, Mo HY, Chen L, et al. A circRNA signature predicts postoperative recurrence in stage II/III colon cancer. EMBO Mol Med. 2019;11:e10168.
10. Huang M, Peng X, Yang L, Yang S, Li X, Tang S, Li B, Jin H, Wu B, Liu J, Li H. Non-coding RNA derived from extracellular vesicles in cancer immune escape: Biological functions and potential clinical applications. Cancer Lett. 2021;501:234–46.
11. Ma Z, Shuai Y, Gao X, Wen X, Ji J. Circular RNAs in the tumour microenvironment. Mol Cancer. 2020;19:8.
12. Hu Z, Chen G, Zhao Y, Gao H, Li L, Yin Y, Jiang J, Wang L, Mang Y, Gao Y, et al. Exosome-derived circCCAR1 promotes CD8 + T-cell dysfunction and anti-PD1 resistance in hepatocellular carcinoma. Mol Cancer. 2023;22:55.
13. Chen DL, Sheng H, Zhang DS, Jin Y, Zhao BT, Chen N, Song K, Xu RH. The circular RNA circDLG1 promotes gastric cancer progression and anti-PD-1 resistance through the regulation of CXCL12 by sponging miR-141-3p. Mol Cancer. 2021;20:166.

14. Shimasaki N, Jain A, Campana D. NK cells for cancer immunotherapy. Nat Rev Drug Discov. 2020;19:200–18.
15. Voskoboinik I, Smyth MJ, Trapani JA. Perforin-mediated target-cell death and immune homeostasis. Nat Rev Immunol. 2006;6:940–52.
16. .Fauriat C, Long EO, Ljunggren HG, Bryceson YT. Regulation of human NK-cell cytokine and chemokine production by target cell recognition. Blood. 2010;115:2167–76.
17. López-Soto A, Gonzalez S, Smyth MJ, Galluzzi L. Control of Metastasis by NK Cells. Cancer Cell. 2017;32:135–54.
18. Hsu J, Hodgins JJ, Marathe M, Nicolai CJ, Bourgeois-Daigneault MC, Trevino TN, Azimi CS, Scheer AK, Randolph HE, Thompson TW, et al. Contribution of NK cells to immunotherapy mediated by PD-1/PD-L1 blockade. J Clin Invest. 2018;128:4654–68.
19. Imai K, Matsuyama S, Miyake S, Suga K, Nakachi K. Natural cytotoxic activity of peripheral-blood lymphocytes and cancer incidence: an 11-year follow-up study of a general population. Lancet. 2000;356:1795–9.
20. Ju HQ, Ying H, Tian T, Ling J, Fu J, Lu Y, Wu M, Yang L, Achreja A, Chen G, et al. Mutant Kras- and p16-regulated NOX4 activation overcomes metabolic checkpoints in development of pancreatic ductal adenocarcinoma. Nat Commun. 2017;8:14437.
21. Lin JF, Hu PS, Wang YY, Tan YT, Yu K, Liao K, Wu QN, Li T, Meng Q, Lin JZ, et al. Phosphorylated NFS1 weakens oxaliplatin-based chemosensitivity of colorectal cancer by preventing PANoptosis. Signal Transduct Target Ther. 2022;7:54.
22. Zheng R, Zhang K, Tan S, Gao F, Zhang Y, Xu W, Wang H, Gu D, Zhu L, Li S, et al. Exosomal circLPAR1 functions in colorectal cancer diagnosis and tumorigenesis through suppressing BRD4 via METTL3-eIF3h interaction. Mol Cancer. 2022;21:49.
23. Seymour L, Bogaerts J, Perrone A, Ford R, Schwartz LH, Mandrekar S, Lin NU, Litière S, Dancey J, Chen A, et al. iRECIST: guidelines for response criteria for use in trials testing immunotherapeutics. Lancet Oncol. 2017;18:e143–52.
24. Gandara DR, Mack PC, Bult C, Li T, Lara PN Jr., Riess JW, Astrow SH, Gandour-Edwards R, Cooke DT, Yoneda KY, et al. Bridging tumor genomics to patient outcomes through an integrated patient-derived xenograft platform. Clin Lung Cancer. 2015;16:165–72.
25. Kawada M, Inoue H, Kajikawa M, Sugiura M, Sakamoto S, Urano S, Karasawa C, Usami I, Futakuchi M, Masuda T. A novel monoclonal antibody targeting coxsackie virus and adenovirus receptor inhibits tumor growth in vivo. Sci Rep. 2017;7:40400.
26. Hegde PS, Chen DS. Top 10 challenges in Cancer Immunotherapy. Immunity. 2020;52:17–35.
27. Yang W, Dong HP, Wang P, Xu ZG, Xian J, Chen J, Wu H, Lou Y, Lin D, Zhong B. IL-36γ and IL-36Ra reciprocally regulate Colon inflammation and tumorigenesis by modulating the Cell-Matrix Adhesion Network and wnt signaling. Adv Sci (Weinh). 2022;9:e2103035.
28. Rowley JW, Chappaz S, Corduan A, Chong MM, Campbell R, Khoury A, Manne BK, Wurtzel JG, Michael JV, Goldfinger LE, et al. Dicer1-mediated miRNA processing shapes the mRNA profile and function of murine platelets. Blood. 2016;127:1743–51.
29. Li K, Wu JL, Qin B, Fan Z, Tang Q, Lu W, Zhang H, Xing F, Meng M, Zou S, et al. ILF3 is a substrate of SPOP for regulating serine biosynthesis in colorectal cancer. Cell Res. 2020;30:163–78.
30. Castella S, Bernard R, Corno M, Fradin A, Larcher JC. Ilf3 and NF90 functions in RNA biology. Wiley Interdiscip Rev RNA. 2015;6:243–56.
31. Brownawell AM, Macara IG. Exportin-5, a novel karyopherin, mediates nuclear export of double-stranded RNA binding proteins. J Cell Biol. 2002;156:53–64.
32. Li X, Liu CX, Xue W, Zhang Y, Jiang S, Yin QF, Wei J, Yao RW, Yang L, Chen LL. Coordinated circRNA Biogenesis and function with NF90/NF110 in viral infection. Mol Cell. 2017;67:214–e227217.
33. Duchange N, Pidoux J, Camus E, Sauvaget D. Alternative splicing in the human interleukin enhancer binding factor 3 (ILF3) gene. Gene. 2000;261:345–53.
34. Bao Y, Zhai J, Chen H, Wong CC, Liang C, Ding Y, Huang D, Gou H, Chen D, Pan Y, et al. Targeting m(6)a reader YTHDF1 augments antitumour immunity and boosts anti-PD-1 efficacy in colorectal cancer. Gut. 2023;72:1497–509.
35. Zhang B, Yao K, Zhou E, Zhang L, Cheng C. Chr20q amplification defines a distinct molecular

subtype of microsatellite stable colorectal Cancer. Cancer Res. 2021;81:1977–87.

36. Ganesh K, Stadler ZK, Cercek A, Mendelsohn RB, Shia J, Segal NH, Diaz LA. Jr.: Immunotherapy in colorectal cancer: rationale, challenges and potential. Nat Rev Gastroenterol Hepatol. 2019;16:361–75.
37. Chen LL. The expanding regulatory mechanisms and cellular functions of circular RNAs. Nat Rev Mol Cell Biol. 2020;21:475–90.
38. Jiang W, Pan S, Chen X, Wang ZW, Zhu X. The role of lncRNAs and circRNAs in the PD-1/PD-L1 pathway in cancer immunotherapy. Mol Cancer. 2021;20:116.
39. Guillerey C, Huntington ND, Smyth MJ. Targeting natural killer cells in cancer immunotherapy. Nat Immunol. 2016;17:1025–36.
40. Zhang PF, Gao C, Huang XY, Lu JC, Guo XJ, Shi GM, Cai JB, Ke AW. Cancer cell-derived exosomal circUHRF1 induces natural killer cell exhaustion and may cause resistance to anti-PD1 therapy in hepatocellular carcinoma. Mol Cancer. 2020;19:110.
41. Gu L, Sang Y, Nan X, Zheng Y, Liu F, Meng L, Sang M, Shan B. circCYP24A1 facilitates esophageal squamous cell carcinoma progression through binding PKM2 to regulate NF-κB-induced CCL5 secretion. Mol Cancer. 2022;21:217.
42. Wang P, Yang W, Guo H, Dong HP, Guo YY, Gan H, Wang Z, Cheng Y, Deng Y, Xie S, et al. IL-36γ and IL-36Ra reciprocally regulate NSCLC progression by modulating GSH Homeostasis and oxidative stress-Induced cell death. Adv Sci (Weinh). 2021;8:e2101501.
43. Wang X, Zhao X, Feng C, Weinstein A, Xia R, Wen W, Lv Q, Zuo S, Tang P, Yang X, et al. IL-36γ transforms the Tumor Microenvironment and promotes type 1 lymphocyte-mediated Antitumor Immune responses. Cancer Cell. 2015;28:296–306.
44. Harusato A, Abo H, Ngo VL, Yi SW, Mitsutake K, Osuka S, Kohlmeier JE, Li JD, Gewirtz AT, Nusrat A, Denning TL. IL-36γ signaling controls the induced regulatory T cell-Th9 cell balance via NFκB activation and STAT transcription factors. Mucosal Immunol. 2017;10:1455–67.
45. Liu CX, Chen LL. Circular RNAs: characterization, cellular roles, and applications. Cell. 2022;185:2016–34.
46. Li P, Mi Q, Yan S, Xie Y, Cui Z, Zhang S, Wang Y, Gao H, Wang Y, Li J, et al. Characterization of circSCL38A1 as a novel oncogene in bladder cancer via targeting ILF3/TGF-β2 signaling axis. Cell Death Dis. 2023;14:59.
47. Xiao L, Zhang Y, Luo Q, Guo C, Chen Z, Lai C. DHRS4-AS1 regulate gastric cancer apoptosis and cell proliferation by destabilizing DHX9 and inhibited the association between DHX9 and ILF3. Cancer Cell Int. 2023;23:304.
48. Liu J, Liu ZX, Li JJ, Zeng ZL, Wang JH, Luo XJ, Wong CW, Zheng JB, Pu HY, Mo HY, et al. The Macrophage-Associated LncRNA MALR facilitates ILF3 liquid-liquid phase separation to promote HIF1α signaling in Esophageal Cancer. Cancer Res. 2023;83:1476–89.
49. Tan J, Sun M, Yin J, Zhou Q, Zhao R, Chen Q, Sun H, Jiang C, Li S, He Y. Hsa_circ_0005050 interacts with ILF3 and affects cell apoptosis and proliferation by disrupting the balance between p53 and p65. Chem Biol Interact. 2022;368:110208.
50. Hu Q, Lu YY, Noh H, Hong S, Dong Z, Ding HF, Su SB, Huang S. Interleukin enhancer-binding factor 3 promotes breast tumor progression by regulating sustained urokinase-type plasminogen activator expression. Oncogene. 2013;32:3933–43.